Effect of Parameter Configuration on Free Vibration of Networked Harmonic Oscillators with Viscous Damping

Xiangdong Liu*

College of Science, Northwest A&F University, Yangling 712100, China

Received: 11.11.2022 & Accepted: 10.02.2023

Doi: 10.12693/APhysPolA.143.326 *e-mail: liuxd@nwafu.edu.cn

Heterogeneous oscillator networks consist of a dynamical function that describes the state of the oscillator (containing several parameters) and a topology that reflects the connections between the oscillators. Revealing the macroscopic dynamics of systems under different configurations of parameters and topology is a topic worthy of discussion and comes with great challenges. In this study, we discuss the effect of different parameter configurations on the damped free vibration of a classical spring oscillator network. On the regular network, we give the analytical expression satisfied by the free vibration of the system under over-damping and critical damping. Furthermore, we discuss the fastest and slowest exponential rates of decay of the system for different parameter conditions. In conjunction with quadratic eigenvalue theory, we extend the above analysis from regular networks to complex networks. We give a general method for calculating the eigenvalue spectrum of the system for arbitrary parameter configurations. In conjunction with the stability of the system and the rate of decay of the exponential rate, we also give numerical simulation results for the second largest and smallest real parts of the eigenvalues of the system. Finally, through the comparative analysis of the simulation results, we relax the matching relationship between the three parameters (mass, damping, and degree) to the matching between two parameters (mass and damping).

topics: parameter configurations, damped free vibration, over-damping, critical damping

1. Introduction

Behind the macroscopic dynamics of the system implicitly is a mechanism for matching the parameters in the function to the topology. Earlier studies on first-order Kuramoto models showed that explosive synchronization (ES) is observed in scale-free networks when the intrinsic frequency of nodes is positively correlated with node degrees [1]. Studies related to ES have resulted in a universal recognition that the rules of organization between parameters and topology underlying the dynamical behavior may be crucial [2–8]. An interesting question is how the dynamics of the system will be determined when the key parameters in the function are placed at important locations in the network. Zhan et al. [9] discussed the vibronic frequencies of classical spring oscillator networks of different masses on complex networks and studied how the mass–space configuration affects the second smallest (ω_2) as well as the largest frequency (ω_N) of the system. Specifically, they studied the undamped second-order system as follows [9]

$$m_j\ddot{x}_j = k\sum_{i=1}^{N} a_{ij}\,(x_i - x_j), \quad j \in 1, 2, \ldots, N, \quad (1)$$

where m_j represents the j-th oscillator's mass; $k = 1$ is the coupling strength (or spring coefficient); N represents the number of mass points (oscillators or nodes); $a_{ij} = 1$ if oscillator i and j are connected, otherwise, $a_{ij} = 0$. Throughout the analysis, all m_j are different. Since (1) can better model the dynamics of proteins in structural biology [10, 11], it has strong practical applications. The authors of [10, 11] found that when the mass of the oscillator is positively correlated with the degree point-to-point, ω_2 is the largest, and ω_N is the smallest. If the oscillator with the smallest degree is given the largest mass (the masses of the other oscillators are arbitrarily assigned), ω_2 is the smallest. In contrast, ω_N is the largest when the oscillator with the largest degree is assigned the lightest mass. Their results also show that the rules of organization between parameters and topology determine the overall dynamics of the system and that even a single node is sufficient to control the collective behavior of the

entire system. Therefore, revealing and effectively using the organization principles of parameters and topology is of significant theoretical and practical significance.

Another important application of the parameter configuration is the synchronization of the grid network. Motter et al. [12] derived the condition for the power-grid network to reach a steady state of synchronization and then used this condition to determine the corresponding adjustable parameters of the generator when the system is spontaneously synchronized [12]. Specifically, the dynamics of generator i is given by the following swing equation

$$\frac{2H_i}{\omega_R}\frac{\mathrm{d}^2\delta_i}{\mathrm{d}t^2} = P_{mi} - P_{ei}, \quad i \in 1, 2, \ldots, N. \tag{2}$$

The parameter H_i is the inertia constant of the generator, ω_R is the reference frequency of the system, P_{mi} is the mechanical power provided by the generator, and P_{ei} is the power demanded of the generator by the network (including the power lost to damping). Note that (2) can be further organized into the following system of equations (the specific symbolic meanings are ignored here, see [12] for details)

$$\dot{Z}_1 = Z_2, \tag{3}$$

$$\dot{Z}_2 = -J\,Z_1 - \Gamma\,Z_2. \tag{4}$$

Here Z_1 and Z_2 are N-dimensional vectors, and T denotes the transpose of the vectors. It is worth noting that in (4), $\Gamma = \beta I$. Here I represents the unit matrix. In other words, in the above analysis, the diagonal elements of Γ are all β. One wonders how a system with damped free vibrations will be determined when the diagonal elements of Γ have arbitrary values in some interval. Here, we study the free vibration of a classical spring oscillator network under viscous damping for different parameter configurations. The innovations of this study are reflected in the following four aspects.

- In contrast to the study by Zhan et al. [9] (see (1)), we have included viscous damping, i.e., we consider the effect of different parameter configurations on the damped free vibration of the system.
- Unlike in the study by Motter et al. [12] (see (4)), the diagonal elements of Γ are no longer identical, but take on arbitrary values within a certain interval.
- For regular networks, we give the analytical expression satisfied by the damped free vibration of the system on a star network. For over-damping and critical damping, we give the smallest and the largest non-zero eigenvalues of the system for different parameter conditions (they determine the degree of exponential rate decay).
- In conjunction with quadratic eigenvalue theory, we extend the above analysis from regular networks to complex networks. A general method for computing the eigenvalue spectrum of the system is given for different parameter-matching schemes. Combined with the system stability, we also give numerical simulation results for the second largest and smallest real part of the system eigenvalues.

The paper is organized as follows. In Sect. 2, we give models of classical spring oscillators of different masses with viscous damping. In Sect. 3, we first give a general expression for the free vibration of the system on a regular network (star network). Furthermore, in Sect. 3.1, for over-damping and critical damping, we give the largest non-zero eigenvalue and the smallest eigenvalue of the system. In conjunction with quadratic eigenvalue theory, in Sect. 3.2, we extend the above study from regular networks to complex networks and give a method for computing the eigenvalue spectrum of a system on a complex network. In Sect. 4, we give numerical simulation results for the second largest $\mathrm{Re}(\lambda_{2N-1})$ and smallest $\mathrm{Re}(\lambda_1)$ real part of the eigenvalues on the Erdös–Rényi (ER) network [13] with different parameter matching schemes. Finally, we summarize and conclude the above research in Sect. 5.

2. Model

We consider the dynamics of N network-coupled classical spring oscillators x_j under the effect of viscous damping, whose evolution is governed by

$$m_j\ddot{x}_j + c_j\dot{x}_j = k\sum_{i=1}^{N} a_{ij}(x_i - x_j), \tag{5}$$

where $j \in 1, 2, \ldots, N$; m_i, x_i, and c_i represent the j-th oscillator's mass, phase, and damping, respectively; $k > 0$ is the coupling strength. For simplicity, we take $k \equiv 1$ throughout the paper. For an undirected graph with no self-loop, $a_{ij} = a_{ji} = 1$ if oscillator j is coupled to oscillator i, otherwise, $a_{ij} = a_{ji} = 0$. Furthermore, m_j and c_j are different for all j in the next analysis. The above equation (5) can be written in a compact form based on the normal mode analysis

$$M\ddot{X} + C\dot{X} + L\,X = 0, \tag{6}$$

where $M = \mathrm{diag}(\{m_j\})$, $C = \mathrm{diag}(\{c_j\})$ and diag denotes the diagonal matrix. The Laplacian matrix is $L = (d_j - \delta_{ij}a_{ij})$, where $\delta_{ij} = 1$ for $i = j$ and $\delta_{ij} = 0$, otherwise; d_j is the degree of node j. For convenience, we denote the mass set $m = (m_1, m_2, \ldots, m_N)$, the damping set $c = (c_1, c_2, \ldots, c_N)$, and the degree vector $d = (d_1, d_2, ..., d_N)$ as m, c, and d, respectively. Next, we consider the solution of (6) in form $X(t) = \mathrm{e}^{\lambda t}U$ and substitute it into (6)

$$\left(\lambda^2\,M + \lambda\,C + L\right)U = 0. \tag{7}$$

We assume that (7) is a quadratic eigenvalue problem (QEP) [14–20], i.e., we determine the scalar $\lambda \in C$ and the non-zero vectors $x, y \in C^N$, such that

$$\left(\lambda^2 M + \lambda C + L\right)x = 0, \tag{8}$$

$$y^H\left(\lambda^2 M + \lambda C + L\right) = 0, \tag{9}$$

where H stands for matrix conjugate transpose; x, y are the left eigenvector and the right eigenvector corresponding to λ, respectively; C represents the complex number field and C^N represents the Cartesian product of N complex number fields. In other words, $X(t) = \mathrm{e}^{\lambda t}U$ is a solution to (6) if and only if λ and U satisfy (8) and (9).

3. Theoretical analysis

3.1. Free vibration of a classical spring oscillator with viscous damping on a star network

Next, we calculate the vibration frequencies of the system on the star network from the perspective of theoretical analysis. From (7) we know that the characteristic polynomial of the system is

$$\mathrm{Det}\begin{pmatrix} \lambda^2 m_1 + \lambda c_1 + (N-1) & -1 & \dots & -1 \\ -1 & \lambda^2 m_2 + \lambda c_2 + 1 & \dots & 0 \\ \vdots & \vdots & \ddots & \vdots \\ -1 & 0 & \dots & \lambda^2 m_N + \lambda c_N + 1 \end{pmatrix} = 0, \tag{10}$$

where Det denotes the determinant of the matrix. When $\lambda^2 m_i + \lambda c_i + 1 = 0$, the $2N-2$ eigenvalues of the system in (10) can be expressed as

$$\lambda_{\pm}^{i} = \frac{-c_i \pm \sqrt{c_i^2 - 4m_i}}{2m_i} \tag{11}$$

for $i \in 2, \dots, N$. Furthermore, the other two eigenvalues of the system are determined by the following implicit expressions

$$\lambda^2 m_1 + \lambda c_1 + (N-1) = \sum_{i=2}^{N} \frac{1}{\lambda^2 m_i + \lambda c_i + 1}. \tag{12}$$

Obviously, $\lambda_{2N} = 0$ is the solution of (12). As for the other solution λ_1, we note the following facts (Viete theorem is used here)

$$\lambda_1 + \lambda_2 + \dots \lambda_{2N} = -\sum_{j=1}^{N} \frac{c_j}{m_j}, \tag{13}$$

thus, we obtain the following result

$$\lambda_1 = -\sum_{j=1}^{N} \frac{c_j}{m_j} - \sum_{k=2}^{N} \frac{-c_k \pm \sqrt{c_k^2 - 4m_k}}{2m_k} = -\frac{c_1}{m_1}. \tag{14}$$

In the next analysis, we assume $c_i^2 \geq 4m_i$ (i.e., over-damping and critical damping situations, see (11)), which means the above $2N-2$ eigenvalues are all real. We can still sort them, i.e., $\lambda_1 \leq \lambda_2 ... \leq \lambda_{2N-1} \leq \lambda_{2N} = 0$. As a result, the general solution of (6) is

$$X(t) = \sum_{k=1}^{2N} c_k \mathrm{e}^{\lambda_k t} U_k, \tag{15}$$

where U_k denotes the eigenvector corresponding to λ_k satisfying (8) and (9). Notice that $e^{\lambda_1 t}$ and $e^{\lambda_{2N-1} t}$ represent the fastest and slowest decay of the exponential rate in the right-hand end of (15) (we exclude the trivial result that $\lambda_{2N} = 0$). In the next analysis, we focus on the two values of λ_1 and λ_{2N-1}. Without loss of generality, we denote the largest of the above $2N-2$ eigenvalues as λ_N^+. This means that $\forall i$ ($i \in 2, \dots, N$, see (11)), the following condition always holds ($\lambda_N^+ \geq \lambda_i^+$)

$$m_N c_i + m_i\sqrt{c_N^2 - 4m_N} > m_i c_N + m_N\sqrt{c_i^2 - 4m_i}. \tag{16}$$

Furthermore, we denote the smallest of the above $2N-2$ eigenvalues as λ_2^-. This means that $\forall i$, ($i \in 2, \dots, N$, see (11)) the following condition always holds ($\lambda_2^- \leq \lambda_i^-$)

$$m_2 c_i + m_i\sqrt{c_2^2 - 4m_2} < m_i c_2 + m_2\sqrt{c_i^2 - 4m_i}. \tag{17}$$

In connection with the previous analysis, if λ_N^+ is the second largest eigenvalue of the whole system (the reader is invited to recall that the largest eigenvalue of the system is 0) and λ_1 is the smallest eigenvalue of the whole system, only the following conditions need to be satisfied ($\lambda_N^+ \geq \lambda_i^+$, $\lambda_2^- \leq \lambda_i^-$, $\lambda_N^+ > \lambda_1$ and $\lambda_2^- > \lambda_1$)

$$\begin{cases} m_N c_i + m_i\sqrt{c_N^2 - 4m_N} > m_i c_N + m_N\sqrt{c_i^2 - 4m_i}, \\ m_2 c_i + m_i\sqrt{c_2^2 - 4m_2} < m_i c_2 + m_2\sqrt{c_i^2 - 4m_i}, \\ m_1 c_N < 2m_N c_1 + m_1\sqrt{c_1^2 - 4m_2}, \\ 2m_2 c_1 < 2m_1 c_2 + m_1\sqrt{c_2^2 - 4m_N}. \end{cases} \tag{18}$$

Similarly, if λ_1 is the second largest eigenvalue of the whole system and λ_2^- is the smallest eigenvalue of the whole system, only the following conditions need to be satisfied ($\lambda_N^+ \geq \lambda_i^+$, $\lambda_2^- \leq \lambda_i^-$ and $\lambda_N^+ < \lambda_1$)

$$\begin{cases} m_N c_i + m_i\sqrt{c_N^2 - 4m_N} > m_i c_N + m_N\sqrt{c_i^2 - 4m_i}, \\ m_2 c_i + m_i\sqrt{c_2^2 - 4m_2} < m_i c_2 + m_2\sqrt{c_i^2 - 4m_i}, \\ m_1 c_N > 2m_N c_1 + m_1\sqrt{c_1^2 - 4m_2}. \end{cases} \tag{19}$$

TABLE I

The mass set m, the damping set c, and the underlying network node degree d point-to-point configuration case. The point-to-point positive (negative) correlation between m and d means that we use $\{m_1/d_1, \ldots, m_N/d_N\}$ ($\{m_N/d_1, \ldots, m_1/d_N\}$) matching when $m_1 < m_2 < \cdots < m_N$, $d_1 < d_2 < \cdots < d_N$. Similarly, the point-to-point positive (negative) correlation between c and d means that we use $\{c_1/d_1, \ldots, c_N/d_N\}$ ($\{c_N/d_1, \ldots, c_1/d_N\}$) matching when $c_1 < c_2 < \cdots < c_N$, $d_1 < d_2 < \cdots < d_N$.

Description	Symbol
m, c are matched with d point-to-point positive correlation	$m \xrightarrow[+]{\text{p.t.p}} d \xleftarrow[+]{\text{p.t.p}} c$
m is positively correlated with d point-to-point, c is negatively correlated with d point-to-point,	$m \xrightarrow[+]{\text{p.t.p}} d \xleftarrow[-]{\text{p.t.p}} c$
m is negatively correlated with d point-to-point, c is positively correlated with d point-to-point,	$m \xrightarrow[-]{\text{p.t.p}} d \xleftarrow[+]{\text{p.t.p}} c$
m, c are matched with d point-to-point negative correlation	$m \xrightarrow[-]{\text{p.t.p}} d \xleftarrow[-]{\text{p.t.p}} c$

Finally, if λ_N^+ is the second largest eigenvalue of the whole system and λ_2^- is the smallest eigenvalue of the whole system, only the following conditions need to be satisfied ($\lambda_N^+ \geq \lambda_i^+$, $\lambda_2^- \leq \lambda_i^-$ and $\lambda_2^- < \lambda_1$)

$$\begin{cases} m_N c_i + m_i\sqrt{c_N^2 - 4m_N} > m_i c_N + m_N\sqrt{c_i^2 - 4m_i}, \\ m_2 c_i + m_i\sqrt{c_2^2 - 4m_2} < m_i c_2 + m_2\sqrt{c_i^2 - 4m_i}, \\ m_1 c_N < 2m_N c_1 + m_1\sqrt{c_1^2 - 4m_2}, \\ 2m_2 c_1 > 2m_1 c_2 + m_1\sqrt{c_2^2 - 4m_N}. \end{cases} \tag{20}$$

3.2. Free vibration of a classical spring oscillator with viscous damping on a complex network

Clearly, $\dot{X} = \lambda \mathrm{e}^{\lambda t} U = \lambda X$ (the reader is invited to recall that we assumed $X = \mathrm{e}^{\lambda t} U$ to be the solution of (7)). We do the following variable substitution

$$z = \begin{pmatrix} x \\ \lambda x \end{pmatrix}, \quad w = \begin{pmatrix} (\lambda M + C)^H y \\ y \end{pmatrix}, \tag{21}$$

$$A = \begin{pmatrix} 0 & I \\ -L & -C \end{pmatrix}, \quad B = \begin{pmatrix} I & 0 \\ 0 & M \end{pmatrix}, \tag{22}$$

where I represents the N-dimensional unit matrix. A direct result is $Az = \lambda Bz$ and $w^H = \lambda w^H B$. Note the following facts

$$A - \lambda B = \begin{pmatrix} 0 & I \\ -I & -\lambda M - C \end{pmatrix} \begin{pmatrix} \lambda^2 M + \lambda C + L & 0 \\ 0 & I \end{pmatrix} \begin{pmatrix} I & 0 \\ -\lambda I & I \end{pmatrix}. \tag{23}$$

In summary, the QEP corresponding to (7) is transformed into a generalized eigenvalue problem (GEP) [21–24]. Notice that $\mathrm{Det}(A - \lambda B) = \mathrm{Det}(\lambda^2 M + \lambda C + L)$. Therefore, the eigenvalues of the GEP are the eigenvalues of the original QEP. This allows us to obtain the full eigenvalues of (7) by numerical computation (the authors used the Cholesky decomposition numerical solution for GEP). It is worth noting that on complex networks, we cannot restrict the eigenvalues of the system (the reader is invited to recall that on the network of rules, we assume that $c_i^2 \geq 4m_i$), which means that we have to address the case of complex eigenvalues. Fortunately, we are concerned with the real part of the eigenvalues of the system from the point of view of system stability. We can still sort them, i.e., $\mathrm{Re}(\lambda_1) \leq \mathrm{Re}(\lambda_2) \cdots \leq \mathrm{Re}(\lambda_{2N-1}) \leq \mathrm{Re}(\lambda_{2N}) \leq 0$ (eigenvalues are pure imaginary numbers). In fact, combined with the general solution of (7) ($X(t) = \sum_{k=1}^{2N} c_k \mathrm{e}^{\lambda_k t} U_k$), when λ_k is a complex number, this means that X contains a linear combination of $\mathrm{e}^{(\alpha_k \pm \mathrm{i}\beta_k)t}$. Thus, X contains a linear combination of $\mathrm{e}^{\alpha_k t}\cos(\beta_k t)$ and $\mathrm{e}^{\alpha_k t}\sin(\beta_k t)$. When $\alpha_k = \mathrm{Re}(\lambda_k) < 0$, each of the above combinations has decayed at an exponential rate. Correspondingly, we are interested in the second largest $\mathrm{Re}(\lambda_{2N-1})$ and smallest $\mathrm{Re}(\lambda_1)$ of the system. In fact, they represent the slowest decay and the fastest decay, respectively.

Before giving specific numerical simulation results on complex networks, we give their notations for different parameter matching schemes. Next, the point-to-point positive (negative) correlation between m and d means that we use $\{m_1/d_1, \ldots, m_N/d_N\}$ ($\{m_N/d_1, \ldots, m_1/d_N\}$) matching when $m_1 < m_2 < \cdots < m_N$, $d_1 < d_2 < \cdots < d_N$. All point-to-point matches of m, c, and d are detailed in Table I. In addition, the single-point positive (negative) correlation between m and d means that we use $\{m_N/d_N\}$ ($\{m_1/d_N\}$) at only one node, while the other nodes are matched in a random way. All single-point matches of m, c, and d are detailed in Table II.

4. Numerical simulations

4.1. Simulation results for $\mathrm{Re}(\lambda_{2N-1})$ with different parameter configurations on ER networks

In Fig. 1a, we give simulation results for $\mathrm{Re}(\lambda_{2N-1})$ under random matching of m and c on the ER network, and the results are arranged in

TABLE II

The mass set m, damping set c, and the underlying network node degree d in a single-point configuration. The single-point positive (negative) correlation between m and d means that we use $\{m_N/d_N\}$ ($\{m_1/d_N\}$) at only one node, while the other nodes are matched in a random way. Similarly, the single-point positive (negative) correlation between c and d means that we use $\{c_N/d_N\}$ ($\{c_1/d_N\}$) at only one node, while the other nodes are matched in a random way.

Description	Symbol
m, c are matched with $d_{\max}$ single-point positive correlation	$m \xrightarrow[+]{\text{s.p}} d_{\max} \xleftarrow[+]{\text{s.p}} c$
m is matched with $d_{\max}$ single-point positive correlation, c is matched with $d_{\max}$ single-point negative correlation,	$m \xrightarrow[+]{\text{s.p}} d_{\max} \xleftarrow[-]{\text{s.p}} c$
m is matched with $d_{\max}$ single-point negative correlation, c is matched with $d_{\max}$ single-point positive correlation,	$m \xrightarrow[-]{\text{s.p}} d_{\max} \xleftarrow[+]{\text{s.p}} c$
m, c are matched with $d_{\max}$ single-point negative correlation	$m \xrightarrow[-]{\text{s.p}} d_{\max} \xleftarrow[-]{\text{s.p}} c$
m, c are matched with $d_{\min}$ single-point positive correlation	$m \xrightarrow[+]{\text{s.p}} d_{\min} \xleftarrow[+]{\text{s.p}} c$
m is matched with $d_{\min}$ single-point positive correlation, c is matched with $d_{\min}$ single-point negative correlation,	$m \xrightarrow[+]{\text{s.p}} d_{\min} \xleftarrow[-]{\text{s.p}} c$
m is matched with $d_{\min}$ single-point negative correlation, c is matched with $d_{\min}$ single-point positive correlation,	$m \xrightarrow[-]{\text{s.p}} d_{\min} \xleftarrow[+]{\text{s.p}} c$
m, c are matched with $d_{\min}$ single-point negative correlation	$m \xrightarrow[-]{\text{s.p}} d_{\min} \xleftarrow[-]{\text{s.p}} c$

ascending order after 50 000 random shuffles (orange). Furthermore, we added two special forms of matching, namely, $m \xrightarrow[+]{\text{p.t.p}} d \xleftarrow[+]{\text{p.t.p}} c$ (red, sphere) and $m \xrightarrow[+]{\text{p.t.p}} d \xleftarrow[-]{\text{p.t.p}} c$ (blue, sphere). We find that the blue sphere is located among the orange lines, while the red sphere is located at the bottom of the whole figure. In other words, compared to random matching, $\mathrm{Re}(\lambda_{2N-1})$ is the smallest under $m \xrightarrow[+]{\text{p.t.p}} d \xleftarrow[+]{\text{p.t.p}} c$.

Similarly, in Fig. 1b, we will give the corresponding results when m is randomly matched with c (orange), $m \xrightarrow[-]{\text{p.t.p}} d \xleftarrow[-]{\text{p.t.p}} c$ (red, sphere), and $m \xrightarrow[-]{\text{p.t.p}} d \xleftarrow[+]{\text{p.t.p}} c$ (blue, sphere). We find that the $\mathrm{Re}(\lambda_{2N-1})$ is minimum when $m \xrightarrow[-]{\text{p.t.p}} d \xleftarrow[-]{\text{p.t.p}} c$. Comparing the blue sphere of Fig. 1a, we find that the value of $\mathrm{Re}(\lambda_{2N-1})$ under $m \xrightarrow[-]{\text{p.t.p}} d \xleftarrow[+]{\text{p.t.p}} c$ becomes the largest (compared to random matching), and the corresponding exponential rate decays the slowest (the reader is invited to recall the relationship between $\mathrm{Re}(\lambda_k)$ and the rate of decay of the exponential rate).

Next, in Fig. 2a, we give the simulation results under parameter single-point matching accordingly. As in Fig. 1a, we give the simulation results for $\mathrm{Re}(\lambda_{2N-1})$ under random matching of m and c (orange), $m \xrightarrow[+]{\text{s.p}} d_{\max} \xleftarrow[+]{\text{s.p}} c$ (red), $m \xrightarrow[+]{\text{s.p}} d_{\max} \xleftarrow[-]{\text{s.p}} c$ (cyan), $m \xrightarrow[+]{\text{s.p}} d_{\min} \xleftarrow[+]{\text{s.p}} c$ (blue), and $m \xrightarrow[+]{\text{s.p}} d_{\min} \xleftarrow[-]{\text{s.p}} c$ (magenta), respectively, and similarly the results are arranged in ascending order after 50 000 random shuffles. We find that the value of $\mathrm{Re}(\lambda_{2N-1})$ under $m \xrightarrow[+]{\text{s.p}} d_{\min} \xleftarrow[-]{\text{s.p}} c$ (magenta) is significantly larger than in the other three cases. Comparing the magenta line with the blue line, we can obviously observe the power of viscous damping (the reader is reminded that in both cases, one is assigned the strongest damping and the other the weakest damping). This also means that the presence of viscous damping accelerates the rate of decay of the exponential rate. Comparing the cyan lines with the red lines, we can reach the same conclusion.

In Fig. 2b, we give the simulation results for $\mathrm{Re}(\lambda_{2N-1})$ under m and c random matching (orange), $m \xrightarrow[-]{\text{s.p}} d_{\max} \xleftarrow[-]{\text{s.p}} c$ (red),$m \xrightarrow[-]{\text{s.p}} d_{\max} \xleftarrow[+]{\text{s.p}} c$ (cyan), $m \xrightarrow[-]{\text{s.p}} d_{\min} \xleftarrow[-]{\text{s.p}} c$ (blue), and $m \xrightarrow[-]{\text{s.p}} d_{\min} \xleftarrow[+]{\text{s.p}} c$ (magenta), respectively, and similarly, the results were arranged in ascending order after 50 000 random shuffles. Comparing Fig. 2a ($m \xrightarrow[+]{\text{s.p}} d_{\min} \xleftarrow[-]{\text{s.p}} c$) with Fig. 2b ($m \xrightarrow[-]{\text{s.p}} d_{\min} \xleftarrow[+]{\text{s.p}} c$), the effect of viscous damping is once again justified. Even though the nodes are assigned different masses, the value of $\mathrm{Re}(\lambda_{2N-1})$ is considerably reduced because the latter is assigned the strongest viscous damping. We are surprised to find that, excluding the top orange line in the figure, the other four color lines almost overlap. In other words, the $\mathrm{Re}(\lambda_{2N-1})$ of the systems of the other four matching methods differ very little, and all are smaller than the values under m and c random matching.

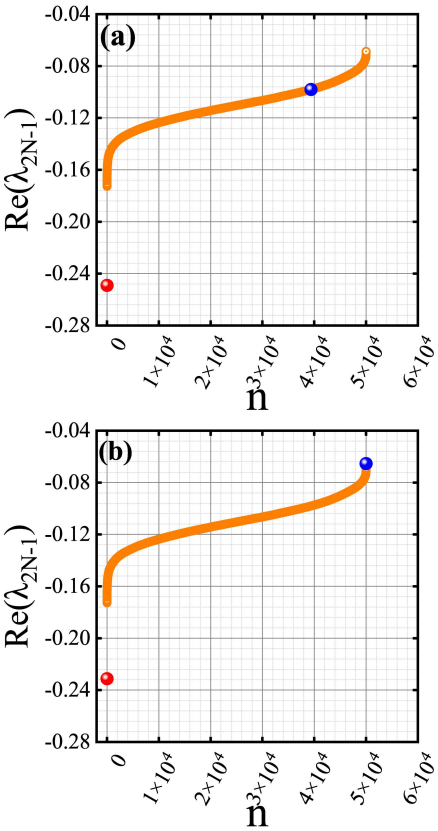

Fig. 1. Effect of parameter point-to-point configuration on $\mathrm{Re}(\lambda_{2N-1})$. The results of $\mathrm{Re}(\lambda_{2N-1})$ under different parameter matching schemes for m, c, and d on Erdös–Rényi (ER) network — (a) $m \xrightarrow[+]{\text{p.t.p}} d \xleftarrow[+]{\text{p.t.p}} c$ (red, sphere), $m \xrightarrow[+]{\text{p.t.p}} d \xleftarrow[-]{\text{p.t.p}} c$ (blue, sphere), random matching of m and c and the results are arranged in ascending order after 50 000 random shuffles (orange); (b) $m \xrightarrow[-]{\text{p.t.p}} d \xleftarrow[-]{\text{p.t.p}} c$ (red, sphere), $m \xrightarrow[-]{\text{p.t.p}} d \xleftarrow[+]{\text{p.t.p}} c$ (blue, sphere), random matching of m and c and the results are arranged in ascending order after 50 000 random shuffles (orange). Here, $N = 50$, $\langle d \rangle = 11.48$ ($\langle d \rangle = (1/N)\sum_{i=1}^{N} d_i$). Here, the mass set ($m$) is taken from a uniform distribution in the range 1–10. The damping set (c) is then taken from a uniform distribution in the range 1–5. Unless specifically mentioned otherwise, throughout the paper these datasets will be used.

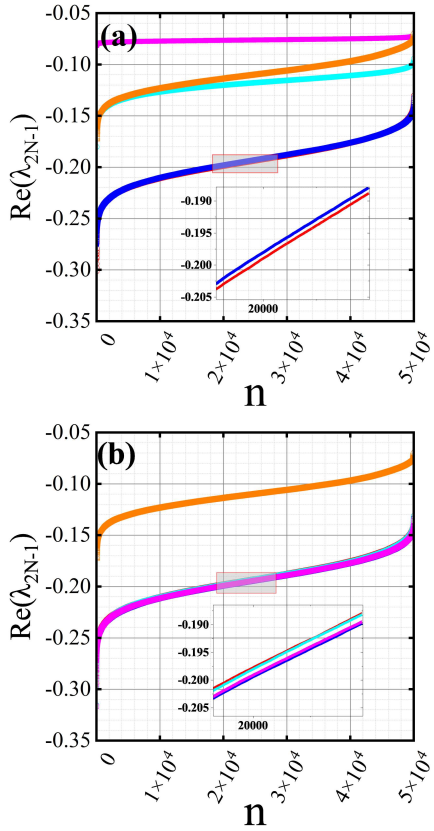

Fig. 2. Effect of parameter single-point configuration on $\mathrm{Re}(\lambda_{2N-1})$. The results of $\mathrm{Re}(\lambda_{2N-1})$ under different parameter matching schemes for m, c, and d on ER network. (a) Random matching of m and c (orange), $m \xrightarrow[+]{\text{s.p}} d_{\max} \xleftarrow[+]{\text{s.p}} c$ (red), $m \xrightarrow[+]{\text{s.p}} d_{\max} \xleftarrow[-]{\text{s.p}} c$ (cyan), $m \xrightarrow[+]{\text{s.p}} d_{\min} \xleftarrow[+]{\text{s.p}} c$ (blue) and $m \xrightarrow[+]{\text{s.p}} d_{\min} \xleftarrow[-]{\text{s.p}} c$ (magenta). All configurations passed a random shuffle of 50 000 and the results are in ascending order. (b) Random matching of m and c (orange), $m \xrightarrow[-]{\text{s.p}} d_{\max} \xleftarrow[-]{\text{s.p}} c$ (red), $m \xrightarrow[-]{\text{s.p}} d_{\max} \xleftarrow[+]{\text{s.p}} c$ (cyan), $m \xrightarrow[-]{\text{s.p}} d_{\min} \xleftarrow[-]{\text{s.p}} c$ (blue), and $m \xrightarrow[-]{\text{s.p}} d_{\min} \xleftarrow[+]{\text{s.p}} c$ (magenta). All configurations passed a random shuffle of 50 000 and the results are in ascending order. Insets are an enlarged version of the shaded area.

Next, let us see if we can relax the matching of the above three parameters ($m \rightarrow d \leftarrow c$) to a match of two parameters ($m \longleftrightarrow c$). In fact, comparing the red sphere in Fig. 1a and b, we find that $\mathrm{Re}(\lambda_{2N-1})$ does not differ much under the two matching schemes. If we further analyze these two matching schemes, we will find that the reason for this phenomenon is actually the positive correlation match between m and c points. Therefore, in Fig. 3a, we ignore the parameter $d_{\min}$ and $d_{\max}$ and directly match m with c in a point-to-point positive correlation (pink sphere) and compare the results with the red sphere in Fig. 1a and b. As we expected, we find that the values of $\mathrm{Re}(\lambda_{2N-1})$ differ very little for the three matches. In fact, the three values in Fig. 2a are $\mathrm{Re}(\lambda_{2N-1}) = -0.249$, -0.235, and -0.231 (from smallest to largest). Similarly, we now consider whether we can relax the single-point matching case. Using the red line and the blue line in Fig. 2a and b, we find that the common feature of these four parameter matching schemes is the single-point positive correlation matching of m with c. Therefore, in Fig. 3b, we directly match m with c in a single-point positive correlation (purple) and compare it with the above

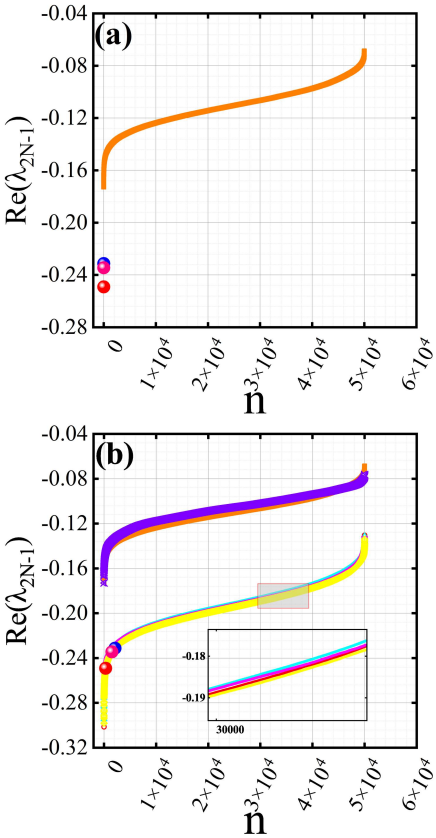

Fig. 3. Relaxation of the configuration between three parameters into a configuration between two parameters. The result of $\mathrm{Re}(\lambda_{2N-1})$ after the above three-parameter match ($m \rightarrow d \leftarrow c$) is relaxed to a two-parameter match ($m \longleftrightarrow c$). (a) Random matching of m and c and the results are arranged in ascending order after 50 000 random shuffles (orange), $m \xrightarrow[+]{\text{p.t.p}} d \xleftarrow[+]{\text{p.t.p}} c$ (red sphere), $m \xrightarrow[-]{\text{p.t.p}} d \xleftarrow[-]{\text{p.t.p}} c$ (blue sphere), and m are positively correlated with c point-to-point (pink sphere). And the above three values are added to Fig. 3b. (b) Random matching of m and c (orange), $m \xrightarrow[+]{\text{s.p}} d_{\max} \xleftarrow[+]{\text{s.p}} c$ (red), $m \xrightarrow[-]{\text{s.p}} d_{\max} \xleftarrow[-]{\text{s.p}} c$ (cyan), $m \xrightarrow[+]{\text{s.p}} d_{\min} \xleftarrow[+]{\text{s.p}} c$ (magenta), $m \xrightarrow[-]{\text{s.p}} d_{\min} \xleftarrow[-]{\text{s.p}} c$ (yellow), and m are positively correlated with c single-point (purple). All configurations passed a random shuffle of 50 000 and the results are in ascending order. Insets are an enlarged version of the shaded area.

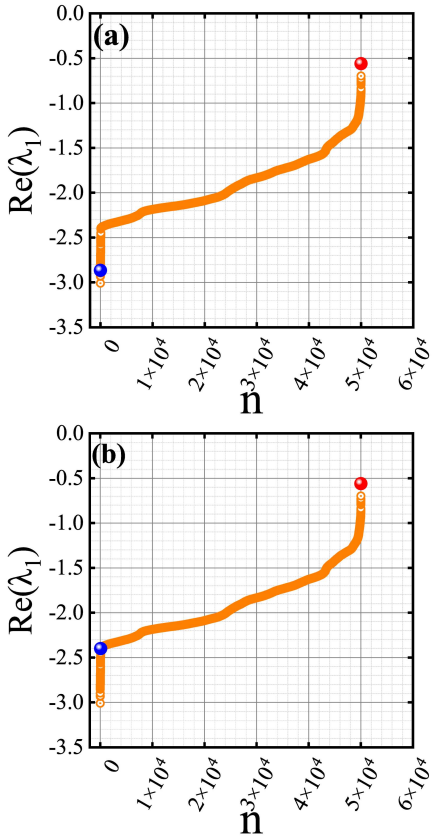

Fig. 4. Effect of parameter point-to-point configuration on $\mathrm{Re}(\lambda_1)$. The results of $\mathrm{Re}(\lambda_1)$ under different parameter matching schemes for m, c, and d on ER network — (a) $m \xrightarrow[+]{\text{p.t.p}} d \xleftarrow[+]{\text{p.t.p}} c$ (red, sphere), $m \xrightarrow[+]{\text{p.t.p}} d \xleftarrow[-]{\text{p.t.p}} c$ (blue, sphere), random matching of m and c and the results are arranged in ascending order after 50 000 random shuffles (orange); (b) $m \xrightarrow[-]{\text{p.t.p}} d \xleftarrow[-]{\text{p.t.p}} c$ (red, sphere), $m \xrightarrow[-]{\text{p.t.p}} d \xleftarrow[+]{\text{p.t.p}} c$ (blue, sphere), random matching of m and c and the results are arranged in ascending order after 50 000 random shuffles (orange).

four matching schemes. We find that the value of $\mathrm{Re}(\lambda_{2N-1})$ also increased substantially if the important parameter d was ignored. On the contrary, if the above pairwise parameter matching ($m \longleftrightarrow c$) is placed on important nodes in the network, such as $d_{\min}$ and $d_{\max}$, the $\mathrm{Re}(\lambda_{2N-1})$ of the system is reduced. The above analysis has significant practical applications. It allows us to obtain the asymptotic minimum of $\mathrm{Re}(\lambda_{2N-1})$ by matching only one pair of parameters under the cost constraint. Furthermore, observing Fig. 3b, we find that the single-point matching produces the global smallest $\mathrm{Re}(\lambda_{2N-1})$.

4.2. Simulation results for $\mathrm{Re}(\lambda_1)$ with different parameter configurations on ER networks

Figure 4 shows the simulation results of the system $\mathrm{Re}(\lambda_1)$ for different matching schemes of m, c, and d on the ER network. Because Fig. 4 uses the same parameter matching scheme as Fig. 1, the marker point shapes and sizes are the same. Therefore, in the discussion that follows, we focus our attention on the results of the simulation experiments rather than a lengthy repetitive narrative. In Fig. 4a and b, we find that the difference is in the case of $\mathrm{Re}(\lambda_{2N-1})$, when the red sphere is located

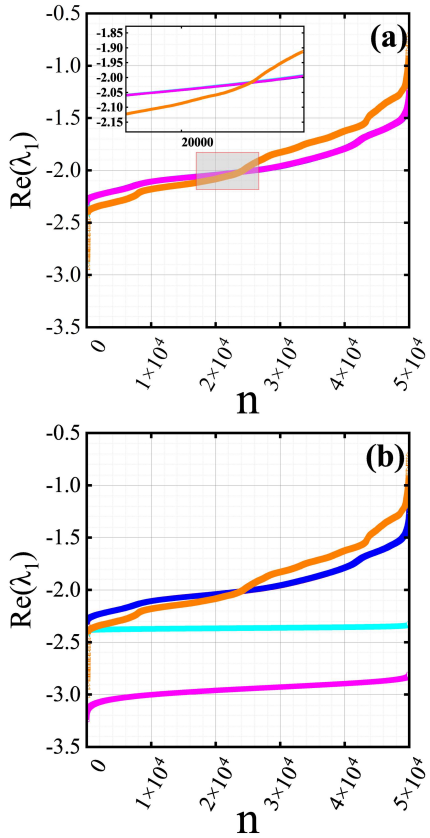

Fig. 5. Effect of parameter single-point configuration on $\mathrm{Re}(\lambda_1)$. The results of $\mathrm{Re}(\lambda_1)$ under different parameter matching schemes for m, c, and d on ER network. (a) Random matching of m and c (orange), $m \xrightarrow[+]{\text{s.p}} d_{\max} \xleftarrow[+]{\text{s.p}} c$ (red), $m \xrightarrow[+]{\text{s.p}} d_{\max} \xleftarrow[-]{\text{s.p}} c$ (cyan), $m \xrightarrow[+]{\text{s.p}} d_{\min} \xleftarrow[+]{\text{s.p}} c$ (blue), and $m \xrightarrow[+]{\text{s.p}} d_{\min} \xleftarrow[-]{\text{s.p}} c$ (magenta). All configurations passed a random shuffle of 50 000 and the results are in ascending order. (b) Random matching of m and c (orange), $m \xrightarrow[-]{\text{s.p}} d_{\max} \xleftarrow[-]{\text{s.p}} c$ (red),$m \xrightarrow[-]{\text{s.p}} d_{\max} \xleftarrow[+]{\text{s.p}} c$ (cyan), $m \xrightarrow[-]{\text{s.p}} d_{\min} \xleftarrow[-]{\text{s.p}} c$ (blue), and $m \xrightarrow[-]{\text{s.p}} d_{\min} \xleftarrow[+]{\text{s.p}} c$ (magenta). All configurations passed a random shuffle of 50 000 and the results in are ascending order. Insets are an enlarged version of the shaded area.

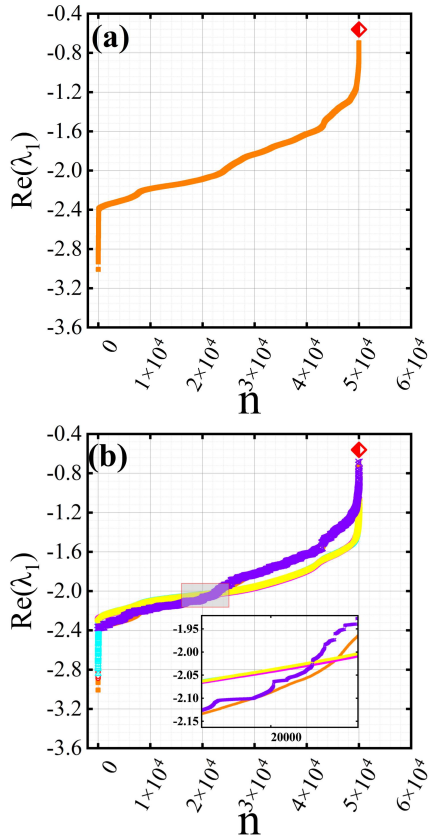

Fig. 6. Relaxation of the configuration between three parameters into a configuration between two parameters. The result of $\mathrm{Re}(\lambda_1)$ after the above three-parameter match ($m \rightarrow d \leftarrow c$) is relaxed to a two-parameter match ($m \longleftrightarrow c$). (a) Random matching of m and c and the results are arranged in ascending order after 50 000 random shuffles (orange), $m \xrightarrow[+]{\text{p.t.p}} d \xleftarrow[+]{\text{p.t.p}} c$, $m \xrightarrow[-]{\text{p.t.p}} d \xleftarrow[-]{\text{p.t.p}} c$, and m are positively correlated with c point-to-point. The three values mentioned above differ so little that we represent them uniformly with a red diamond and add them to the Fig. 6b. (b) Random matching of m and c (orange), $m \xrightarrow[+]{\text{s.p}} d_{\max} \xleftarrow[+]{\text{s.p}} c$ (red), $m \xrightarrow[-]{\text{s.p}} d_{\max} \xleftarrow[-]{\text{s.p}} c$ (cyan), $m \xrightarrow[+]{\text{s.p}} d_{\min} \xleftarrow[+]{\text{s.p}} c$ (magenta), $m \xrightarrow[-]{\text{s.p}} d_{\min} \xleftarrow[-]{\text{s.p}} c$ (yellow), and m are positively correlated with c single-point (purple). All configurations passed a random shuffle of 50 000 and the results are in ascending order. Insets are an enlarged version of the shaded area.

at the top of the figure. The blue sphere, on the other hand, is located in the middle of the orange line. This means that the $\mathrm{Re}(\lambda_1)$ is maximum when $m \xrightarrow[+]{\text{p.t.p}} d \xleftarrow[+]{\text{p.t.p}} c$ and $m \xrightarrow[-]{\text{p.t.p}} d \xleftarrow[-]{\text{p.t.p}} c$ (compared to random matching). Correspondingly, the exponential rate decays the slowest. Next, we discuss the simulation results of the parameters under the corresponding single-point matching. In Fig. 5a, we find that, excluding the orange color line, the other four color lines (red, cyan, magenta, and blue) almost overlap. In Fig. 5b, we find that the magenta line ($m \xrightarrow[-]{\text{s.p}} d_{\min} \xleftarrow[+]{\text{s.p}} c$) is located at the bottom of the figure. Comparing the magenta line with the blue line, we find that the strong viscous damping effect also reduces the value of $\mathrm{Re}(\lambda_1)$ substantially. Similarly, comparing the red and cyan lines, the same conclusion can be drawn.

In Fig. 6a, we give the results for $\mathrm{Re}(\lambda_1)$ under m and c point-to-point positive correlation matching. Comparing the three-parameter matching cases

of $m \xrightarrow[+]{\text{p.t.p}} d \xleftarrow[+]{\text{p.t.p}} c$, $m \xrightarrow[-]{\text{p.t.p}} d \xleftarrow[-]{\text{p.t.p}} c$, we find that the difference of $\mathrm{Re}(\lambda_1)$ in the system is very small. As the differences between the three values above are small, we have used a red diamond to represent them uniformly in the figure. In fact, the three values in Fig. 6a are $\mathrm{Re}(\lambda_1) = -0.55992$, -0.55979, and -0.55976 (from smallest to largest). Also, in Fig. 6b we compare the $\mathrm{Re}(\lambda_1)$ under m and c random matching (orange), m and c single-point positive correlation (purple), $m \xrightarrow[+]{\text{s.p}} d_{\max} \xleftarrow[+]{\text{s.p}} c$ (red), $m \xrightarrow[-]{\text{s.p}} d_{\max} \xleftarrow[-]{\text{s.p}} c$ (cyan), $m \xrightarrow[+]{\text{s.p}} d_{\min} \xleftarrow[+]{\text{s.p}} c$ (magenta), and $m \xrightarrow[-]{\text{s.p}} d_{\min} \xleftarrow[-]{\text{s.p}} c$ (yellow). We find that the difference between the $\mathrm{Re}(\lambda_{2N-1})$ case, the $\mathrm{Re}(\lambda_1)$ under $m \longleftrightarrow c$ and $m \rightarrow d \leftarrow c$, is not significant. Furthermore, we find that the $\mathrm{Re}(\lambda_1)$ are globally maximal under $m \xrightarrow[-]{\text{p.t.p}} d \xleftarrow[-]{\text{p.t.p}} c$.

5. Conclusions

In this study, we discuss the effect of parameter configurations on the free vibration of a harmonic oscillator network under the effect of viscous damping. On the star network, our calculation gives the analytical expression satisfied by the free vibration of the system under viscous damping (15). We focused on the smallest and the largest non-zero eigenvalues of the system, which represent the fastest and the slowest decay of the exponential rate in (15). For the over-damped and critically damped cases, our classification discussion traverses all the cases where the above two eigenvalues are taken for different parameter conditions. In conjunction with quadratic eigenvalue theory, we have successfully generalized the above analysis to complex networks. Throughout our analysis, the selection of parameters in the system is arbitrary, thus generalizing the work of Motter et al. [12] in grid networks. By transforming the QEP problem into a GEP problem, our theoretical analysis gives a general method for capturing all eigenvalues of (5) on complex networks. In connection with the relationship between system eigenvalues and stability and exponential rate decay, we studied the variation of $\mathrm{Re}(\lambda_1)$ and $\mathrm{Re}(\lambda_{2N-1})$ for all matching schemes (including point-to-point and single-point matching) between m, c, and d. A summary analysis of the numerical simulation results gives us the following results:

(i) we find that a single-point matching of m, c with d produces the smallest $\mathrm{Re}(\lambda_{2N-1})$ (see Fig. 3b);

(ii) for $m \xrightarrow[+]{\text{p.t.p}} d \xleftarrow[+]{\text{p.t.p}} c$ and $m \xrightarrow[-]{\text{p.t.p}} d \xleftarrow[-]{\text{p.t.p}} c$, we can relax the matching between three parameters ($m \rightarrow d \leftarrow c$) to the matching between two parameters ($m \longleftrightarrow c$) (see Fig. 3a and Fig. 6a);

(iii) comparing $m \xrightarrow[+]{\text{s.p}} d_{\min} \xleftarrow[-]{\text{s.p}} c$ with $m \xrightarrow[+]{\text{s.p}} d_{\min} \xleftarrow[+]{\text{s.p}} c$, we find that the value of $\mathrm{Re}(\lambda_{2N-1})$ is greatly reduced by the strong viscous damping effect (see Fig. 2a);

(iv) we find that m, c, and d point-to-point matching produces the largest $\mathrm{Re}(\lambda_1)$ (see Fig. 6b).

Vibration is a common form of motion in engineering and technology [25–29]. The study of vibration problems can be modeled as a second-order system [30, 31]. In our study, we studied the effect of different configurations of parameters on the vibration of the system, where all parameters are taken arbitrarily. This means that we cannot decouple the system, as was the case in the study by Motter et al. [12], which makes the study considerably more challenging. This is why on complex networks we can only study $\mathrm{Re}(\lambda_{2N-1})$ and $\mathrm{Re}(\lambda_1)$ by numerical simulation. In fact, (6) has a wide range of practical applications as an abstract second-order system. These applications include but are not limited to the fields of spontaneous synchronization of generators in power grids [12], protein structure dynamics [32], and vibration control [33, 34]. Next, we will consider the impact of external drivers [35, 36]. How the parameter configuration affects the system with damped forced vibrations is still an open question. We also expect our research to generate general interest in parameter-topology-dynamics.

Data are available on request from the authors.

References

[1] J. Gomez-Gardenes, S. Gómez, A. Arenas, Y. Moreno, *Phys. Rev. Lett.* **106**, 128701 (2011).

[2] H. Chen, G. He, F. Huang, C. Shen, Z. Hou, *Chaos* **23**, 033124 (2013).

[3] M.M. Danziger, O.I. Moskalenko, S.A. Kurkin, X. Zhang, S. Havlin, S. Boccaletti, *Chaos* **26**, 065307 (2016).

[4] V. Avalos-Gaytan, J. A. Almendral, I. Leyva, F. Battiston, V. Nicosia, V. Latora, S. Boccaletti, *Phys. Rev. E* **97**, 042301 (2018).

[5] N. Lotfi, F. A. Rodrigues, A. H. Darooneh, *Chaos* **28**, 033102 (2018).

[6] I. Leyva, I. Sendina-Nadal, S. Boccaletti, *Discrete Continuous Dyn. Syst. B* **23**, 1931 (2018).

[7] S. Jalan, A. Kumar, I. Leyva, *Chaos* **29**, 041102 (2019).

[8] X. Ling, W.-B. Ju, N. Guo, C.-Y. Wu, X.-M. Xu, *Phys. Lett. A* **384**, 126881 (2020).

[9] M. Zhan, S. Liu, Z. He, *PloS one* **8**, e82161 (2013).

[10] Q. Cui, I. Bahar, *Normal Mode Analysis: Theory and Applications to Biological and Chemical Systems*, CRC press, 2005.

[11] I. Bahar, T.R. Lezon, A. Bakan, I.H. Shrivastava, *Chem. Rev.* **110**, 1463 (2010).

[12] A.E. Motter, S.A. Myers, M. Anghel, T. Nishikawa, *Nat. Phys.* **9**, 191 (2013).

[13] P. Erdös, A. Rényi, *Publ. Math. Inst. Hung. Acad. Sci* **5**, 17 (1960).

[14] F. Tisseur, K. Meerbergen, *SIAM Rev.* **43**, 235 (2001).

[15] C.-H. Guo, P. Lancaster, *Math. Comput.* **74**, 1777 (2005).

[16] M.S. Misrikhanov, V. N. Ryabchenko, *Autom. Remote Control* **67**, 698 (2006).

[17] P. Lancaster, I. Zaballa, *Mech. Syst. Signal Process.* **23**, 1134 (2009).

[18] S. Hammarling, C.J. Munro, F. Tisseur, *ACM Trans. Math. Software* **39**, 1 (2013).

[19] X. Hou, Y. Su, Z. Zuo, X. Dai, Y. Fei, *IEEE Trans. Power Electron.* **36**, 9907 (2021).

[20] J. Sadet, F. Massa, T. Tison, I. Turpin, B. Lallemand, E.-G. Talbi, *Mech. Syst. Signal Process.* **153**, 107492 (2021).

[21] G.W. Stewart, *Math. Comput.* **29**, 600 (1975).

[22] M. Chugunova, D. Pelinovsky, *J. Math. Phys.* **51**, 052901 (2010).

[23] B. Ghojogh, F. Karray, M. Crowley, arXiv:1903.11240, 2019.

[24] J.-M. Liang, S.-Q. Shen, M. Li, S.-M. Fei, *Quantum Inf. Process.* **21**, 1 (2022).

[25] F. Casciati, G. Magonette, F. Marazzi, *Technology of Semiactive Devices and Applications in Vibration Mitigation*, John Wiley & Sons, 2006.

[26] B. Wen, *Front. Mech. Eng. China* **3**, 1 (2008).

[27] N. Baisheng, L. Xiangchun, *Saf. Sci.* **50**, 741 (2012).

[28] M.S. Jaballah, S. Harzallah, B. Nail, *Eng. Technol. Appl. Sci. Res.* **12**, 8652 (2022).

[29] B. Wen, X. Huang, Y. Li, Y. Zhang, *Vibration Utilization Engineering*, Springer, 2022, p. 57.

[30] A. Azimi, F. Bakhtiari-Nejad, W. Zhu, *J. Franklin Inst.* **358**, 6545 (2021).

[31] J. Awrejcewicz, G. Sypniewska-Kaminska, O. Mazur, *Mech. Syst. Signal Process.* **163**, 108132 (2022).

[32] I. Bahar, T.R. Lezon, A. Bakan, I.H. Shrivastava, *Chem. Rev.* **110**, 1463 (2010).

[33] J. Danielson, J. Lawrence, W. Singhose, *J. Dyn. Syst. Meas. Control* **130**, 556 (2008).

[34] A. Dhanda and G. Franklin, in: *Proc. 2005, American Control Conf., Portland (OR)*, 2005, p. 3574.

[35] H. Zhu, W. Zhu, W. Fan, *J. Sound Vib.* **491**, 115759 (2021).

[36] X. Chen, D. Peng, J. Hu, C. Li, S. Zheng, W. Zhang, *Proc. Inst. Mech. Eng. D J. Automobile Eng.* **236**, 2219 (2022).